Articles

Neurology

11-25-2018

Diet-induced insulin resistance elevates hippocampal glutamate as well as VGLUT1 and GFAP expression in AβPP/PS1 mice.

Erin R Hascup

Sarah O Broderick

Mary K Russell

Yimin Fang

Andrzej Bartke

See next page for additional authors

Follow this and additional works at: https://opensiuc.lib.siu.edu/neurology_articles

Authors

Erin R Hascup, Sarah O Broderick, Mary K Russell, Yimin Fang, Andrzej Bartke, Heather A Boger, and Kevin N Hascup

ORIGINAL ARTICLE

Diet-induced insulin resistance elevates hippocampal glutamate as well as VGLUT1 and GFAP expression in AβPP/PS1 mice

Erin R. Hascup*†, Sarah O. Broderick*, Mary K. Russell‡, Yimin Fang§, Andrzej Bartke§, Heather A. Boger‡ and Kevin N. Hascup* (iD)

*Department of Neurology, Center for Alzheimer's Disease and Related Disorders, Neurosciences Institute, Springfield, Illinois, USA

†Department of Pharmacology, Southern Illinois University School of Medicine, Springfield, Illinois, USA

‡Department of Neuroscience, Center on Aging, Medical University of South Carolina, Charleston, South Carolina, USA

§Division of Geriatric Research, Department of Internal Medicine, Southern Illinois University School of Medicine, Springfield, Illinois, USA

Abstract

The symptomologies of Alzheimer's disease (AD) develop over decades suggesting modifiable lifestyle factors may contribute to disease pathogenesis. In humans, hyperinsulinemia associated with type 2 diabetes mellitus increases the risk for developing AD and both diseases share similar age-related etiologies including amyloidogenesis. Since we have demonstrated that soluble $A\beta_{42}$ elicits glutamate release, we wanted to understand how diet-induced insulin resistance alters hippocampal glutamate dynamics, which are important for memory formation and consolidation. Eight to twelve-week-old C57BL/6J and AβPP/PS1 mice were placed on either a low-fat diet or high-fat diet (HFD) for 8 months. A HFD led to significant weight increases as well as impaired insulin sensitivity, glucose tolerance, and learning in both C57BL/6J and AβPP/PS1 mice. AβPP/PS1 low-fat diet mice had elevated hippocampal basal as well as stimulus-evoked glutamate release that was further increased with consumption of a HFD. Immunohistochemistry indicated an increase in vesicular glutamate transporter 1 and glial fibrillary acidic protein density in hippocampal subregions corresponding with this elevated extracellular glutamate. While no differences in hippocampal plaque load were observed, the elevated astrogliotic response surrounding the plaques in AβPP/PS1 HFD mice may have been a compensatory mechanism to control plaque accumulation. These data support that AβPP/PS1 mice have chronically elevated extracellular glutamate that is exacerbated by a HFD and that modifiable lifestyle factors such as obesity-induced insulin resistance can contribute to AD pathogenesis.

Keywords: Alzheimer's disease, amyloid-beta, astrogliosis, cognition, diabetes, excitotoxicity.

J. Neurochem. (2018) https://doi.org/10.1111/jnc.14634

ORIGINAL ARTICLE

Alzheimer's disease (AD) is an age-related neurodegenerative disorder characterized by a slow, but progressive, accumulation of extracellular aggregated beta-amyloid (Aβ) and intracellular hyperphosphorylated tau tangles (Jack *et al.* 2013). This accumulation leads to alterations in neurotransmitter dynamics, synapse loss, and cerebral atrophy that culminate in the eventual cognitive and functional decline associated with the disorder (Mota *et al.* 2014). To date, current therapeutics target cholinesterase inhibitors, to increase acetylcholine levels, or antagonism of the N-methyl-D-aspartate (NMDA) receptor, to prevent glutamate-mediated excitotoxicity (Cummings *et al.* 2014; Godyń *et al.* 2016). However, these therapies have limited efficacy, only treat symptoms, and do not decelerate disease progression, possibly because they are administered at advanced AD stages. Without a well-established biomarker for AD, early diagnosis is difficult and underscores the lack of disease-modifying pharmacotherapy options. To further complicate diagnosis, evidence supports that AD symptomology develops over decades and modifiable lifestyle factors, such as obesity-induced type 2 diabetes mellitus (T2DM), may contribute to AD progression (Barnes and Yaffe 2011).

The peptide hormone, insulin, regulates glucose uptake and storage in the periphery and brain for use in energy production (Felice 2013). However, excessive caloric consumption, particularly of hydrogenated or saturated fats, promotes a cascade of metabolic events starting with elevated circulating insulin concentrations that leads to insulin resistance and increases the risk factor for developing T2DM (Holland *et al.* 2007). In fact, T2DM and AD share several age-related etiologies including hyperinsulinemia, insulin resistance, hyperglycemia, amyloidogenesis, and memory impairment (Zhao and Townsend 2009; Talbot *et al.* 2012; Moloney *et al.* 2010). These similar symptomologies suggest insulin resistance and the subsequent onset of T2DM is a risk for developing AD (Vandal *et al.* 2014). In support of this, the Mayo Clinic Alzheimer Disease Patient Registry has reported that 80% of their AD patients had either T2DM or impaired glucose tolerance (Janson *et al.* 2004) and T2DM in midlife increases the odds for developing mild cognitive impairment or AD later in life by 1.5- to 2-fold (Allen *et al.* 2004; Ott *et al.* 1999; Arvanitakis *et al.* 2004). While the mechanistic link between T2DM and AD is not fully elucidated, the metabolic hypothesis of AD which supports altered insulin signaling promotes a cascade of neurological events that initiate the pathogenesis of AD (Hoyer 2002). For example, brain insulin-degrading enzyme (IDE) regulates the metabolism of both insulin and Aβ, but at a lower affinity for the latter. As such, hyperinsulinemia prevents IDE from degradation of monomeric Aβ leading to its accumulation and aggregation (Farris *et al.* 2003). These small molecular weight isoforms of Aβ (monomers, dimers, and trimers) are hypothesized to be the bioactive component that causes synaptic dysfunction, neurotoxicity, and the eventual neurodegeneration associated with AD (Jin and Selkoe 2015; Yang *et al.* 2017).

Prior studies have demonstrated that soluble $Aβ_{42}$ elicits glutamate release through the α7 nicotinic acetylcholine receptor (α7nAChR; Talantova *et al.* 2013; Hascup and Hascup 2016). Because of glutamate's role in learning and memory, it is hypothesized that persistent, excessive synaptic glutamate overstimulates the NMDA receptor thereby preventing the detection of physiological signals leading to cognitive impairment (Parsons *et al.* 2007). In fact, our laboratory has demonstrated that double transgenic mice expressing a mutant amyloid precursor protein (Mo/HuAPP695swe) and Presenilin 1 (PS1-dE9) genes (AβPP/PS1) have elevated hippocampal glutamate as early as 2–4 months of age, prior to the onset of cognitive decline (Hascup and Hascup 2015). While previous studies have demonstrated that HFD exacerbates cognitive decline and disease neuropathology in animal models of AD (Vandal *et al.* 2014; Knight *et al.* 2014; Thériault *et al.* 2016; Julien *et al.* 2010), alterations to memory-associated neurotransmitters have not been elucidated. The aim of the present study was to address how obesity-induced insulin resistance alters glutamate dynamics in both cognitively normal and AβPP/PS1 mice predisposed to AD pathology. Since previous studies have shown that HFD affects memory in cognitively normal rodents (Kanoski and Davidson 2011; Cordner and Tamashiro 2015), non-AD control mice help to understand changes associated with, or independent from, the metabolic hypothesis of AD pathogenesis.

Materials and methods

Animals

Protocols for animal use were approved by the *Laboratory Animal Care and Use Committee* at Southern Illinois University School of Medicine (Protocol #219-14-003) and the study was not preregistered. Eight- to twelve-week-old male, C57BL/6J (RRID: IMSR_JAX:000664) and AβPP/PS1 (RRID:MMRRC_034832-JAX; Mo/HuAPP695swe/PS1-dE9), mice were obtained from Jackson Laboratory (Bar Harbor, ME, USA), and group housed on a 12:12-h light: dark cycle with food and water available *ad libitum*. All experiments were conducted during the light phase. Genotype was confirmed by TransnetYX®, Inc (Cordova, TN, USA). All mice were ear tagged with unique numerical identifiers so as to blind researchers throughout the experimental paradigms. Pseudorandomization using the Microsoft Excel 2013 randomization function to generate random decimal numbers between 0 and 1 for each mouse and dietary treatment. These random numbers were then sorted into ascending order generating a list that categorized mice into the following groups: C57BL/6J low-fat diet (LFD), C57BL/6J HFD, AβPP/PS1 LFD, and AβPP/PS1 HFD. Similar methodology was used to determine the order of which animals were assessed. A $n = 15$ for all treatment groups was allocated at study initiation; however, due to animal loss from normal aging and disease progression, the following indicates the remaining number of animals available at the end of the 8-month dietary treatment:

C57BL/6J LFD ($n = 14$), C57BL/6J HFD ($n = 11$), AβPP/PS1 LFD ($n = 11$), and AβPP/PS1 HFD ($n = 12$). All of these remaining mice underwent blood glucose monitoring, cognitive assessment, *in vivo* glutamate recordings, and immunohistochemical (IHC) analysis except for one AβPP/PS1 HFD mouse that died during *in vivo* glutamate recordings as outlined in Fig. 1a. Following *in vivo* electrochemistry, all mice were killed by an overdose of isoflurane followed by rapid decapitation with sharp scissors.

Chemicals

All chemicals were prepared and stored according to manufacturer recommendations unless otherwise noted. L-glutamate oxidase (EC 1.4.3.11) was obtained from Cosmo Bio USA Co. (Carlsbad, CA, USA; Cat: YMS-80049) and reconstituted in distilled, deionized water to make a 1 U/µL stock solution and stored at 4°C. Sodium phosphate monobasic monohydrate (Cat: BP330-500), sodium phosphate dibasic anhydrous (Cat: S375-500), 1,3-phenylenediamine
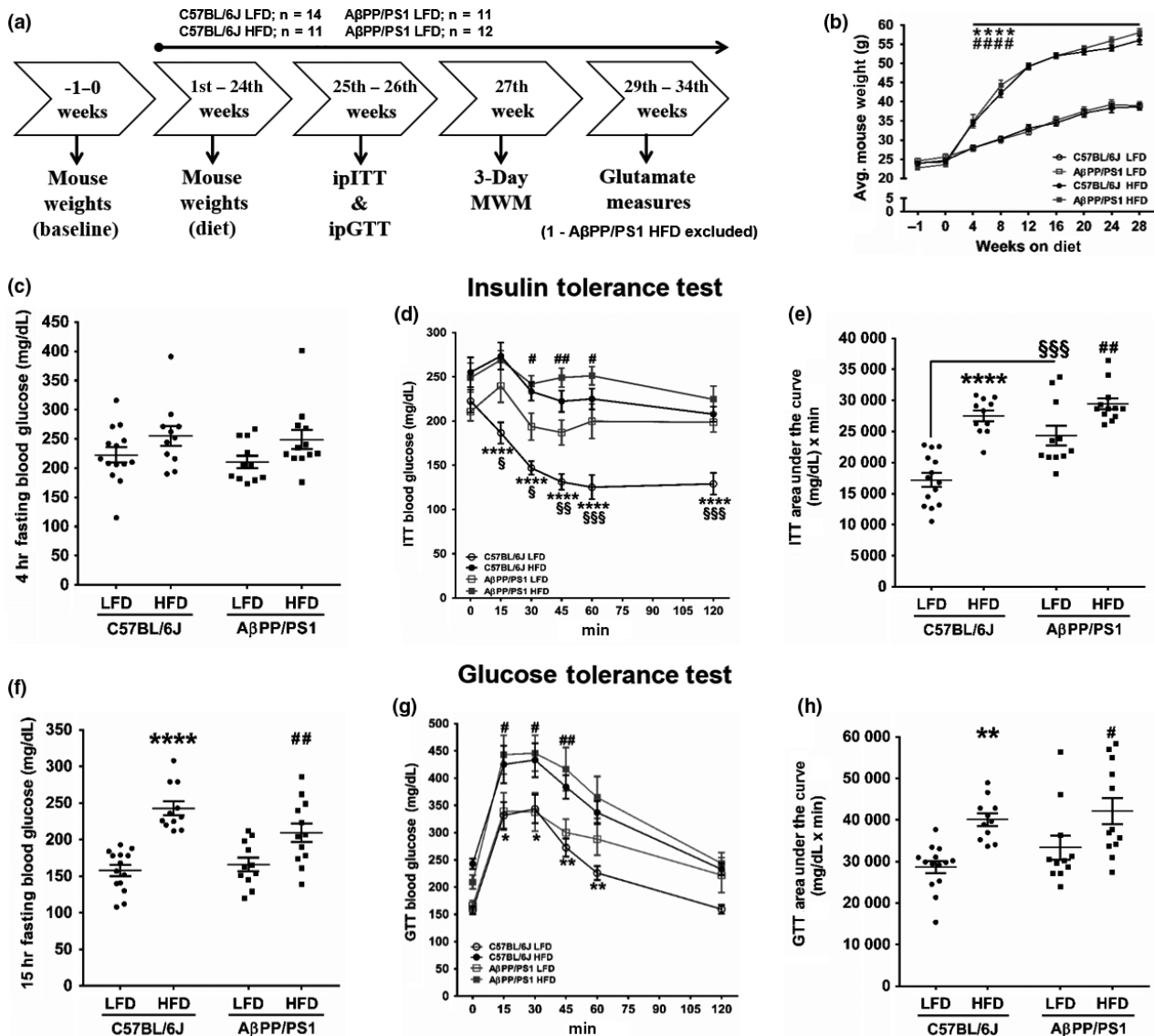
Fig. 1 Experimental design, mouse weight, and blood glucose measurements. (a) An outline of the experimental design. Abbreviations: intraperitoneal insulin tolerance test (ipITT), intraperitoneal glucose tolerance test (ipGTT), Morris water maze (MWM). (b) Analysis of mouse weight gain through 28 weeks on either LFD or high-fat diet (HFD). Results from the 4-h fasting ipITT and 15-h fasting ipGTT. Mouse genotypes and diet group are indicated on each graph. (c) Four-hour fasting blood glucose prior to ip injection of 1 IU/kg b.w. of insulin, (d) blood glucose during the 120-min ipITT, (e) area under the curve of the 120-min ipITT, (f14-h fasting blood glucose prior to ip injection of 2 g/kg b.w. of glucose, (g) blood glucose during the 120-min ipGTT, (h) area under the curve of the 120-min ipGTT. *$p < 0.05$, **$p < 0.01$, ****$p < 0.0001$ C57BL/6J LFD ($n = 14$) versus C57BL/6J HFD ($n = 11$); #$p < 0.05$, ##$p < 0.01$, ####$p < 0.0001$ AβPP/PS1 LFD ($n = 11$) versus AβPP/PS1 HFD ($n = 12$); §$p < 0.05$, §§$p < 0.01$, §§§$p < 0.001$ C57BL/6J LFD versus AβPP/PS1 LFD; where n refers to the number of animals.

dihydrochloride (mPD; Cat: P017225G), sodium chloride (Cat: S271-3), calcium chloride dehydrate (Cat: BP510-100), dextrose monohydrate (Cat: D15-500), and hydrogen peroxide (H_2O_2; Cat: H325-100) were obtained from Thermo Fisher Scientific (Waltham, MA, USA). L-glutamic acid sodium salt (Cat: G1626), potassium chloride (Cat: P9333), bovine serum albumin (BSA; Cat: A3059), glutaraldehyde (Cat: G5882), dopamine hydrochloride (DA; Cat: H8502), L-ascorbic acid (AA; Cat: A7056), and dibutyl phthalate and xylene (Cat: 06522) were obtained from Sigma-Aldrich Co. (St. Louis, MO, USA). Rabbit polyclonal glial fibrillary acidic protein (GFAP) antibody was obtained from Dako (Carpinteria, CA, USA; RRID:AB_10013382). Guinea pig polyclonal vesicular glutamate transporter 1 (VGLUT1) antibody was obtained from Millipore (Burlington, MA, USA; RRID: AB_2301751). Biotinylated goat anti-rabbit serum (RRID: AB_2313606), biotinylated goat anti-guinea pig serum (RRID: AB_2336132), avidin–biotin complex kit (RRID:AB_236818), and VIP peroxidase substrate kit (RRID:AB_2336819) were obtained from Vector Laboratories (Burlingame, CA, USA). Amylo-Glo® RTD™ with ethidium bromide (EtBr) was obtained from Biosensis (Temecula, CA, USA; Cat: TR-400-AG).

Low–fat and high–fat diet

All mice were switched from standard rodent chow (13% kcal fat, 57% kcal carbohydrate, 30% kcal protein, 4% sucrose, 4.09 kcal/gm; LabDiet; Cat: 5001) to either a LFD (10% kcal fat, 70% kcal carbohydrate, 20% kcal protein, 7% sucrose, 3.85 kcal/gm; Cat: D12450J) or a HFD (60% kcal fat, 20% kcal carbohydrate, 20% kcal protein, 7% sucrose, 5.24 kcal/gm; Cat: D12492) obtained from Research Diets Inc. (New Brunswick, NJ, USA). A LFD diet was used as the control diet so as to match protein and sucrose content with the HFD. Mouse weight was monitored throughout the study (Fig. 1b).

Intraperitoneal insulin tolerance test (ITT) and glucose tolerance test (GTT)

To determine insulin sensitivity, an initial blood glucose measurement (time = 0) was taken from the tail vein of 4-h fasted mice and measured using a Presto® glucometer (AgaMatrix, Salem, NH, USA) followed by intraperitoneal (ip) injection of 1 IU/kg body weight (b.w.) Humulin® R (Henry Schein, Melville, NY, USA: Cat: 1238578). To determine glucose tolerance, an initial blood glucose measurement was taken (time = 0) from 15-h fasted mice followed by an ip injection of 2 g of glucose/kg b.w. Following either injection, blood glucose levels were measured sequentially at 15, 30, 45, 60, and 120 min (Fang *et al.* 2017).

Morris water maze

The morris water maze (MWM) paradigm consisted of two consecutive training days where the mouse learned to remain on the platform for 60 s before rescue. For the first training day, a visible platform protruded 1 cm out of the opaque pool of water to aid in platform location. Mice underwent three consecutive 60-s maximum trials with a 15-min intertrial interval. On the second training day, the visible platform was removed and mice underwent three training blocks (30-min interblock interval) of 3, 60-s maximum trials (15-min intertrial interval) to learn the location of the submerged platform (1 cm below the surface). Starting quadrant was varied for each trial. The probe challenge consisted of a single 60-s trial. The ANY-maze video tracking system (Stoelting Co.,

Wood Dale, IL, USA; RRID:SCR_014289) records and analyzes maze navigation. The three training sessions for Day 1 and for each training block in Day 2 were averaged.

Enzyme–based microelectrode arrays

Enzyme-based MEAs with platinum (Pt) recording surfaces were fabricated, assembled, coated, and calibrated for *in vivo* mouse glutamate measurements as previously described (Burmeister *et al.* 2000; Hascup *et al.* 2006, 2013). One of the MEA (Quanteon LLC; Cat: R2) Pt sites was coated with an L-glutamate oxidase, BSA, glutaraldehyde solution. BSA and glutaraldehyde increase the adhesion and crosslink L-glutamate oxidase to the MEA surface, while L-glutamate oxidase enzymatically degrades glutamate to α-ketoglutarate and H_2O_2, the electroactive reporter molecule. The second Pt recording site (self-referencing or sentinel site) was coated with a BSA and glutaraldehyde solution that is unable to enzymatically generate H_2O_2 from L-glutamate. A potential of +0.7V versus a Ag/AgCl reference electrode was applied to the Pt recording surfaces, resulting in a two electron oxidation of H_2O_2, and the subsequent current was amplified and digitized by the fast analytical sensing technology 16mkIII (Quanteon, LLC; Nicholasville, KY) electrochemistry instrument.

mPD Electropolymerization

Pt recording surfaces were electroplated with 5 mM mPD in 0.05 M phosphate-buffered saline for 20 min to restrict the passage of AA, DA, uric acid, and 3,4-dihydroxyphenylacetic acid (Hascup *et al.* 2016).

Calibration

MEAs were calibrated in 0.05 M phosphate-buffered saline (37°C) to create a standard curve for the conversion of current to glutamate concentration. Final beaker concentrations of 250 μM AA, 20, 40, and 60 μM L-glutamate, 2 μM DA, and 8.8 μM H_2O_2 were used to assess MEA performance. A total of 49 MEAs were used in the present study. The average ± standard error of the mean (SEM) for glutamate sensitivity was 5.7 ± 0.3 pA/μM ($R^2 = 0.998 \pm 0.001$), selectivity ratio of 367 ± 48 to 1, and limit of detection of 0.20 ± 0.03 μM based on a signal-to-noise ratio of 3.

In Vivo anesthetized recordings

A glass micropipette (World Precision Instruments, Inc.; Cat: 1B100-6) was used for local application studies. The tip of the micropipette (12–15 μm internal diameter) was positioned between the pair of recording sites and mounted ~100 μm above the MEA surface. Mice were anesthetized using 1.5% isoflurane (Henry Schein; Cat: 029405) in a calibrated vaporizer (Parkland Scientific; V3000) and placed in a stereotaxic frame with a mouse anesthesia mask (David Kopf Instruments; Cat: 900/907). Body temperature was maintained at 37°C. The MEA/micropipette assembly was lowered into the dentate gyrus (DG; AP: −2.0, ML: ± 1.0, DV: −2.2 mm), CA3 (AP: −2.0, ML: ± 2.0, DV: −2.2 mm), and CA1 (AP: −2.0, ML: ± 1.0, DV: −1.7 mm) from Bregma (Paxinos and Franklin 2004). A Ag/AgCl reference wire was positioned beneath the skull and rostral to the right hemisphere craniotomy. Constant voltage amperometry (4 Hz) was performed

using the fast analytical sensing technology 16mkIII. Calibration data in conjunction with a MATLAB (MathWorks, Natick, MA, USA; RRID:SCR_014289) graphic user interface program (Version 6.1) was used to calculate extracellular glutamate. The sentinel site current (pA) was subtracted from the glutamate recording site current (pA) and divided by the slope (pA/μM) obtained during the calibration (Burmeister and Gerhardt 2001; Burmeister *et al.* 2002; Hascup *et al.* 2010, 2011).

Immunohistochemistry and semi–quantification

Following *in vivo* electrochemistry, the brains were removed and post-fixed in 4% paraformaldehyde for 48 h and then transferred into 30% sucrose in 0.1 M PB for 24 h prior to sectioning. Forty-five micron sections of the hippocampus were obtained using a Microm cryostat (Zeiss; Cat: HM 500). Serial sections (every sixth) of the hippocampus were processed for free-floating immunohistochemistry (IHC) using rabbit polyclonal GFAP (1 : 2000) or guinea pig polyclonal VGLUT1 antibody (1 : 1000) (Farrand *et al.* 2017; Hascup *et al.* 2016). Endogenous peroxidase activity was quenched by treating sections with 10% H_2O_2 in 20% methanol for 10 min. Sections for primary antibodies were permeabilized in Tris-buffered saline with 0.25% TritonX-100 following treatment for 20 min with sodium metaperiodate. Nonspecific binding was controlled by 1-h incubation in 10% normal goat serum. Sections were incubated overnight in the primary antibody at 23°C. The next day, sections were incubated for 1 h with the secondary antibody (1 : 200; biotinylated goat anti-rabbit serum or biotinylated goat anti-guinea pig serum) and 1 h with the Vectastain avidin–biotin complex kit (Vector). The reaction was developed using the VIP peroxidase substrate kit (Vector) to enhance the reaction and produce a color stain. This reaction was stopped using 0.1 M PB, and the sections were mounted on glass slides, dehydrated, and coverslipped with dibutyl phthalate and xylene. To control for staining intensity, staining of all sections for each antibody was conducted on the same day and developed with VIP for the same amount of time (GFAP: 3 min, VGLUT1: 2 min). For plaque staining, slides containing serial sections (every sixth) of the hippocampus were incubated for 10 min in freshly prepared Amylo-Glo® RTD™ solution followed by a 5-min rinse in 0.9% saline without shaking, then 1-min incubation with EtBr based on product protocol (1 : 100). Staining intensities of GFAP, VGLUT1, and plaque formation in the hippocampus were determined using National Institutes of Health Image J Software 1.48 (RRID:SCR_003070) to measure a gray scale value within the range of 0–256, where 0 represents white and 256 represents black (Farrand *et al.* 2017). A template for the DG, CA3, and CA1 hippocampal subregions was created for VGLUT1 and GFAP while a template for the whole hippocampus was created for plaque formation. Templates were used on all brains similarly, and images were captured with a Nikon Eclipse E-600 microscope equipped with an Olympus-750 video camera system and a Dell Pentium III computer. Measurements were performed blinded, and approximately six sections were averaged to obtain one value per subject. If six sections per stain were not obtained, the subject was excluded from data analysis. Staining density was obtained when background staining was subtracted from mean staining intensities on every sixth section through the hippocampus.

Aβ42 ELISA

A separate cohort of mice was used for insoluble $A\beta_{42}$ determination. Mice were killed as described above and the hippocampus was dissected and stored at −80°C until tissue processing. Protein concentrations were determined using the bicinchoninic acid method, and the assessment of the insoluble fractions of $A\beta_{42}$ was performed using the Human/Rat β amyloid (42) ELISA kit (WAKO Chemicals; Cat: 292-64501).

Data analysis

Sample size was determined based on previous MWM, electrochemical, and IHC data using C57BL/6J and AβPP/PS1 mice. A power calculation indicated a minimum of 10 mice per group for MWM and electrochemical recordings and five mice per group for IHC analysis (Boger *et al.* 2007; Hascup and Hascup 2015) to detect differences with 95% confidence (α = 0.05) and 0.8 power. Prism (GraphPad Software, Inc., La Jolla, CA, USA; RRID: SCR_002798) software was used for all statistical analyses including D'Agostino-Pearson omnibus normality tests. A one-way analysis of variance (ANOVA) was used for MWM and for electrochemical stimulus volume comparisons, while a two-way ANOVA (diet vs genotype) was used for all other analyses. When the ANOVA indicated a statistically significant main effect, a Holm-Sidak's multiple comparisons post hoc test was used. Outliers were determined with a single Grubb's test (α = 0.05). Data are represented as mean ± SEM and significance was defined as $p < 0.05$. The unit of analysis 'n' for each dataset refers to the number of mice and data are available upon request.

Results

Changes in weight gain induced by a HFD

An outline of the experimental design is presented in Fig. 1a. All mice were given a 2-week acclimation period when they arrived at our animal facility, placed on standard chow for 2 weeks, and weighed weekly until study completion (Fig. 1b). Following the 2-week acclimation period, pseudorandomization was used to assign mice to either the C57BL/6J LFD (n = 14), C57BL/6J HFD (n = 11), AβPP/PS1 LFD (n = 11), or AβPP/PS1 HFD (n = 12) groups. All mice remained on their respective diets until study completion. A diet effect was observed at 4 weeks (F[3, 44] = 81.29; $p < 0.0001$). As expected, both C57BL/6J and AβPP/PS1 mice on HFD gained more weight compared to genotype-matched LFD groups No differences in weight gain were observed between genotypes within each diet group.

HFD impairs peripheral insulin sensitivity

After 24 weeks on their respective diets, the effects of a HFD on the sensitivity of blood glucose levels to the action of insulin were tested with an ipITT. No difference in blood glucose levels was observed during a 4-h fast (Fig. 1c). A HFD significantly impaired peripheral insulin sensitivity compared to genotype-matched LFD mice when examining the 120-min blood glucose response to the insulin challenge

$(F[3, 44] = 23.58; p < 0.0001;$ Fig. 1d) as well as the subsequent area under the curve analysis $(F[1, 44] = 45.41; p < 0.0001;$ Fig. 1e) indicating an obesity-induced T2DM phenotype. Additionally, an effect of genotype $(F[1, 44] = 15.61; p = 0.0003)$ was observed supporting that AβPP/PS1 mice have impaired insulin sensitivity that is independent of diet (Fig. 1d and e).

Glucose metabolism is impaired in mice fed a HFD

The effects of a HFD on glucose metabolism were tested using the ipGTT. Mice fed a HFD had significantly $(F[1, 44] = 42.28; p < 0.0001;$ Fig. 1f) elevated 15 h fasting blood glucose compared to genotype-matched LFD mice as a result of the obesity-induced insulin resistance. Mice fed a HFD-metabolized glucose slower during the 120-min glucose challenge $(F[3, 44] = 8.019; p = 0.0002)$ and subsequent area under the curve analysis $(F[1, 44] = 18.32; p < 0.0001)$ compared to genotype-matched LFD mice (Fig. 1g and h).

Mice on a HFD have impaired spatial learning and memory

One week following ipGTT and 27 weeks into dietary feeding, mice underwent a 3-day MWM. The MWM tests spatial learning and memory recall by requiring the mouse to utilize visual cues to repeatedly swim to a static, submerged platform, regardless of the starting quadrant. During the MWM, mice were trained to locate a visible escape platform on Day 1 and a hidden platform on Day 2. The visible platform verifies visual acuity while simultaneously habituating the mice to the novel environment thereby reducing

stress while encouraging a motivation to escape the pool (Gulinello *et al.* 2009). The three training sessions for Day 1 and for each training block in Day 2 were averaged for individual mice for analysis. Latency to reach to the platform as well as cumulative distance from the platform was assessed. Cumulative distance is a proximity measure designed to reflect search error through summation of the distance from the platform calculated at 1-s intervals while accounting for trial variations in starting quadrant and swimming speed (Gallagher *et al.* 2015). As shown in Fig. 2a, AβPP/PS1 HFD took longer to locate the hidden escape platform during the first training block of Day 2 compared to their Day 1 performance $(F[3, 44] = 4.118; p = 0.0117)$. In Fig. 2b, C57BL/6J LFD mice were the only group that did not travel further from the hidden escape platform on the first training block of Day 2 and continued to significantly decrease over successive training blocks $(F[3, 52] = 3.449; p = 0.0231)$ compared to their Day 1 performance. On the contrary, the other three groups of mice traveled further from the hidden escape platform on the first training block of Day 2, which was significant in AβPP/PS1 HFD mice $(F[3, 44] = 5.178; p = 0.0038)$ compared to their Day 1 performance. While C57BL/6J HFD and both AβPP/PS1 diet groups decreased the cumulative distance from the hidden escape platform over successive training blocks, a significant improvement over Day 1 performance was not observed supporting decreased learning in these three groups of mice. During the MWM probe challenge for memory recall, no differences were observed in the number of annulus 40 crossings (Fig. 2c).
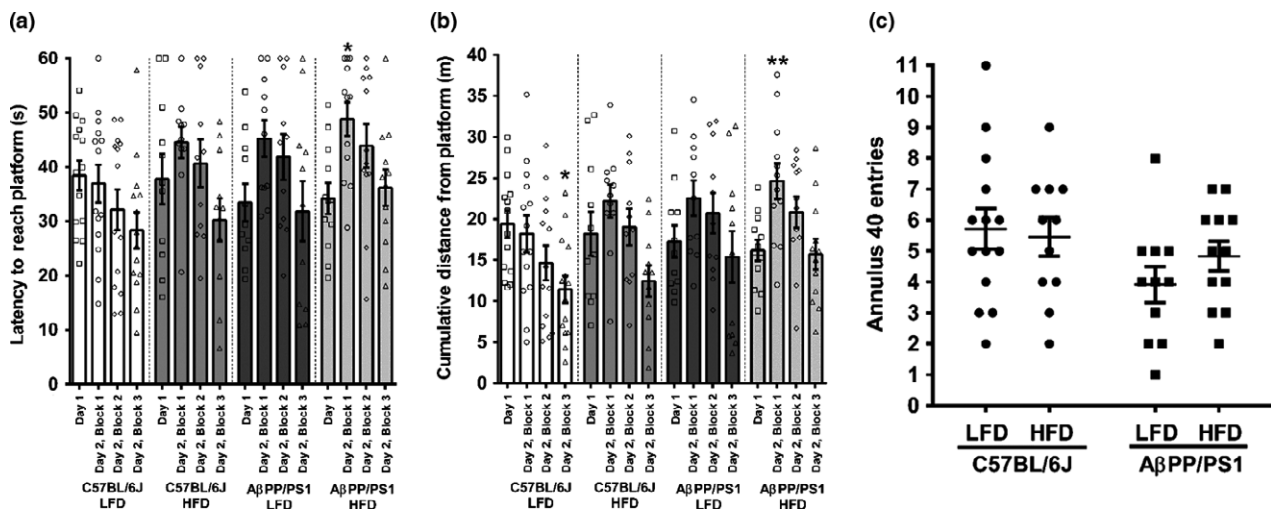
Fig. 2 MWM Training and Probe Challenge. The 2-day MWM training session consisted of a visible platform on Day 1 that was changed to a hidden platform on Day 2 and the probe challenge. (a) Latency to reach the escape platform for each training session. (b) The cumulative distance each mouse spent away from the platform for the training sessions. A & B) *$p < 0.05$, **$p < 0.01$, hidden platform versus Day 1 visible platform. (c) The number of annulus 40 crossings. C57BL/6J LFD, $n = 14$; C57BL/6J high-fat diet (HFD), $n = 11$; AβPP/PS1 LFD, $n = 11$; AβPP/PS1 HFD, $n = 12$; where n refers to the number of animals.

HFD elevates hippocampal basal glutamate

A minimum of 2-week post-MWM (29 weeks into dietary feeding) an enzyme-based MEA was used to measure glutamate dynamics in the DG, CA3, and CA1. Representative glutamate traces showing basal and stimulus-evoked glutamate release are presented in Fig. 3. Basal glutamate was calculated by taking a 10-s baseline average prior to the start of pressure ejection in the DG, CA3, and CA1. When examining basal glutamate (Fig. 4a–c), a genotype effect was only observed in the CA1 ($F[1, 43] = 12.23$; $p = 0.0011$), indicating increased tonic glutamate in AβPP/PS1 mice. A diet effect was observed in the DG ($F[1, 43] = 6.232$; $p = 0.0165$), CA3 ($F[1, 43] = 12.90$; $p = 0.0008$), and CA1 ($F[1, 43] = 12.78$; $p = 0.0009$), supporting that a HFD elevates basal glutamate with synergistic effects observed in AβPP/PS1 mice.

HFD alters hippocampal glutamate dynamics

A glass micropipette attached to the enzyme-based MEA was used to locally apply sterile filtered (0.20 μm) 70 mM KCl (70 mM KCl, 79 mM NaCl and 2.5 mM CaCl$_2$, pH 7.4) by pressure ejection (5–15 psi, 1–2 s pulses) using a Picospritzer III (Parker-Hannafin Corp.). Ejection volumes were maintained between 100 and 200 nl in each hippocampal subfield and monitored using a stereomicroscope (Luxo Corp. Cat:, Elmsford, NY, USA) fitted with a calibrated reticule (Hascup and Hascup 2016). Similar volumes of stimulus were locally applied in the DG ($F[3, 40] = 0.7720$; $p = 0.5165$), CA3 ($F[3, 40] = 0.3397$; $p = 0.7967$), and CA1 ($F[3, 41] = 1.655$; $p = 0.1915$) of all mouse groups to elicit glutamate release (Fig. 4d–f). A genotype effect was observed in the DG ($F[1,40] = 8.429$; $p = 0.0060$), CA3 ($F[1, 40] = 4.720$; $p = 0.0358$), and CA1 ($F[1, 41] = 7.559$;
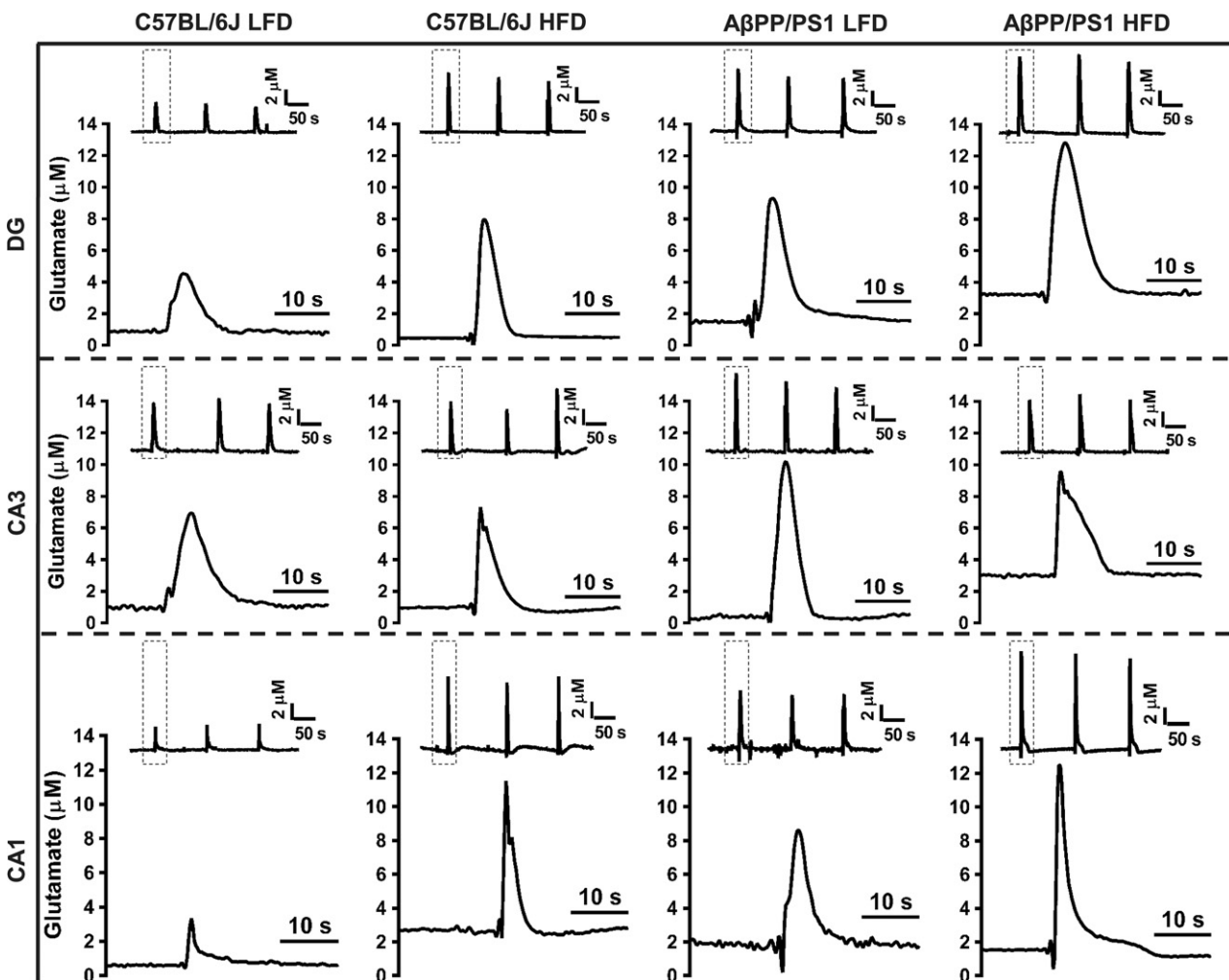
Fig. 3 Stimulus-evoked glutamate release traces. Representative traces of glutamate release from 70 mM KCl stimulation. Columns indicate genotype and diet while rows indicate hippocampal subfield. Within each panel, the inset trace depicts the reproducibility of the glutamate signals with the dashed box indicating a single response magnified beneath for a clearer presentation of glutamate dynamics. Concentration and time axes are consistent in all panels for comparative interpretation.
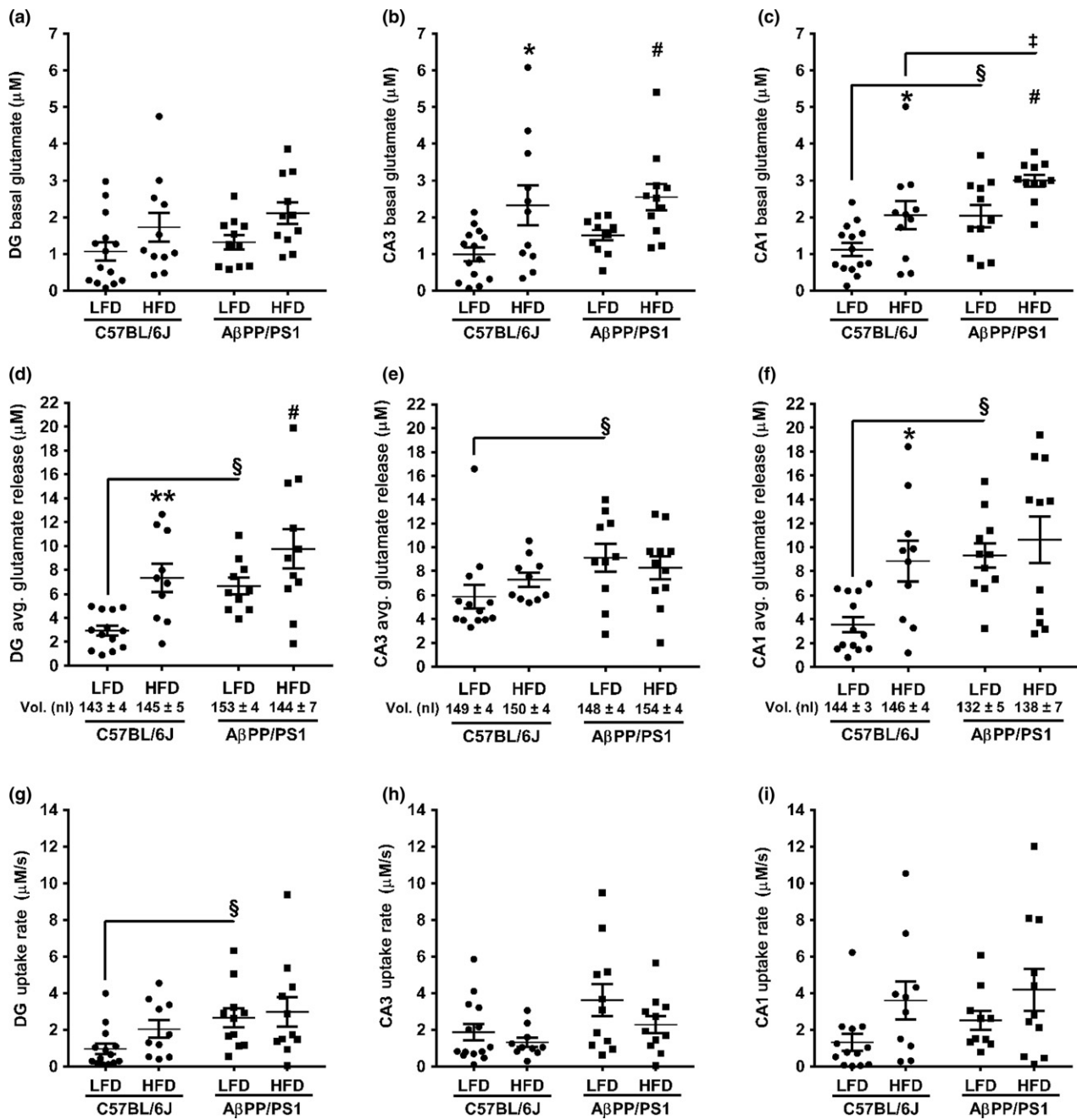
Fig. 4 Hippocampal Glutamate Measures. Basal glutamate, stimulus-evoked glutamate release, and evoked glutamate uptake rate in the DG (a, d, g), CA3 (b, e, h), and CA1 (c, f, i). Basal glutamate was measured prior to local application of stimulus. Stimulus volumes (mean $\pm$ SEM) are shown beneath the bar graphs in (d–f). *$p < 0.05$, **$p < 0.01$ C57BL/6J LFD ($n = 13$–14; one subject excluded) versus C57BL/6J high-fat diet (HFD) ($n = 10$–11; one subject excluded);

[#]$p < 0.05$ AβPP/PS1 LFD ($n = 10$–11; one subject excluded) versus AβPP/PS1 HFD ($n = 11$; one subject died); [§]$p < 0.05$ C57BL/6J LFD ($n = 13$–14) versus AβPP/PS1 LFD ($n = 10$–11); [‡]$p < 0.05$ C57BL/6J HFD ($n = 10$) versus AβPP/PS1 HFD ($n = 11$); where n refers to the number of animals and at most a single subject per group was excluded by Grubb's test.

$p = 0.0088$), whereby AβPP/PS1 mice release more glutamate upon depolarization. A diet effect was observed in the DG ($F[1, 40] = 12.57$, $p = 0.0010$) and CA1 ($F[1, 41] = 5.772$; $p = 0.0209$), but not the CA3 ($F[1, 40] = 0.0870$; $p = 0.7695$), indicating a HFD increased stimulus-evoked glutamate release. The clearance of glutamate is predominantly mediated by uptake in high-efficiency excitatory amino acid transporters (EAAT) located on glia

(Zhou and Danbolt 2013). A significant effect of genotype was observed for glutamate uptake rate in the DG ($F[1, 42] = 6.050$; $p = 0.0181$) and CA3 ($F[1, 42] = 5.793$; $p = 0.0206$), but not the CA1 (Fig. 4g–i). A significant effect from diet led to increased glutamate uptake rate only in the CA1 ($F[1, 40] = 5.721$; $p = 0.0216$).

Increased expression of VGLUT1 in HFD mice

IHC was used to determine changes in VGLUT1 expression in the DG, CA3, and CA1. Representative images of VGLUT1 from the DG are shown in Fig. 5a–d ($40\times$ magnification) and average mean density for each hippocampal subfield is presented in Fig. 5e–g. A significant effect of genotype on VGLUT1 expression was observed in the DG ($F[1, 34] = 12.40$; $p = 0.0012$), CA3 ($F[1, 33] = 12.59$; $p = 0.0012$), and CA1 ($F[1, 36] = 32.74$; $p < 0.0001$), supporting that the elevated hippocampal basal and stimulus-evoked glutamate release in APP/PS1 mice is a result of increased glutamatergic vesicles. Likewise, a significant effect of diet existed on VGLUT1 expression in the DG ($F[1, 34] = 17.67$; $p = 0.0002$), CA3 ($F[1, 33] = 27.63$; $p < 0.0001$), and CA1 ($F[1, 36] = 17.54$; $p = 0.0002$), indicating that a HFD increased glutamatergic vesicles corresponding with the elevated hippocampal glutamate.

GFAP expression is increased by HFD

IHC was used to determine changes in GFAP expression in the DG, CA3, and CA1. Whole hippocampal representative images ($10\times$ magnification) of GFAP expression are shown in Fig. 6a–d and average mean density for each hippocampal subfield is presented in Fig. 6e–g. A significant effect of genotype on GFAP expression was observed in the DG ($F[1, 36] = 14.83$; $p = 0.0005$), CA3 ($F[1, 37] = 23.07$; $p < 0.0001$), and CA1 ($F[1, 39] = 100.60$; $p < 0.0001$), as indicated by greater hippocampal GFAP expression in APP/PS1 mice. In addition, a significant effect of diet exists on GFAP expression in the C57BL/6J DG ($F[1, 36] = 9.006$; $p = 0.0049$) and AβPP/PS1 CA3 ($F[1, 37] = 20.13$; $p < 0.0001$) and CA1 ($F[1, 39] = 15.98$; $p = 0.0003$), indicating that a HFD results in greater astrogliosis.

A HFD does not alter plaque formation

Hippocampal plaque formation was determined by staining with Amylo-Glo® RTD™. Whole hippocampal representative images ($10\times$ magnification) of plaque accumulation (blue) and EtBr counter-stain (red) are shown in Fig. 7a–d and average mean density of whole hippocampal plaque accumulation is presented in Fig. 7e. As indicated by the arrows in Fig. 7c and d, a genotype effect caused increased
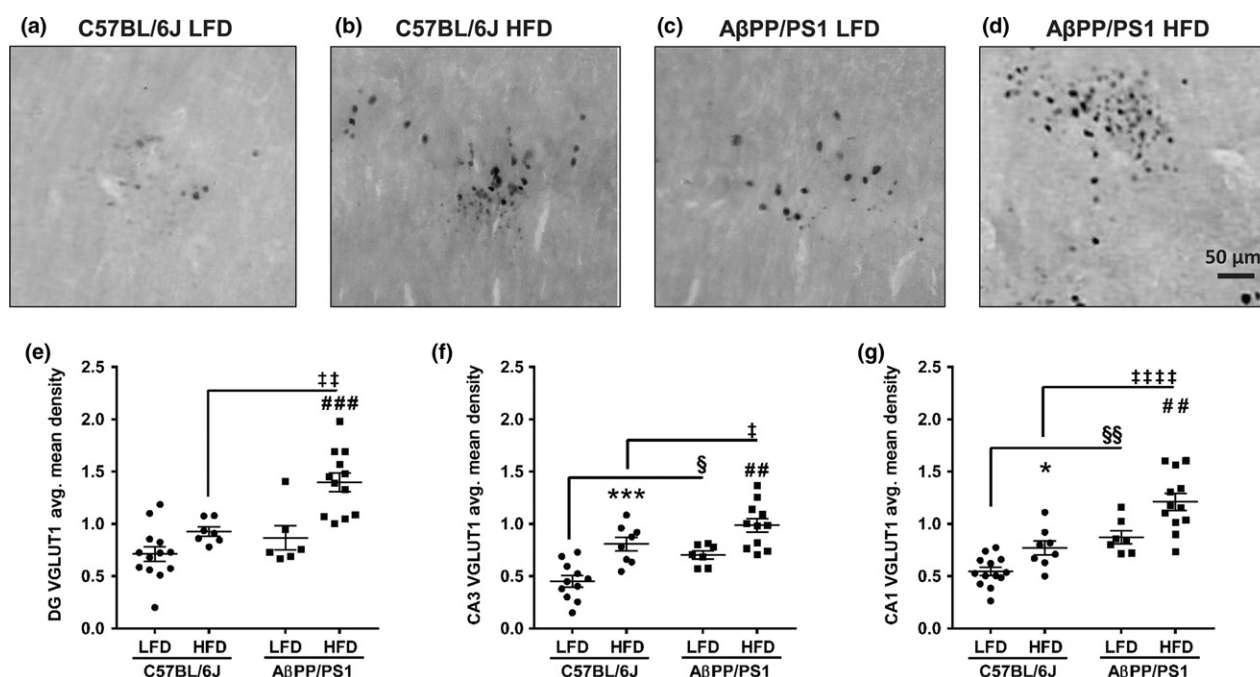
Fig. 5 VGLUT1 Immunohistochemistry. Representative images of VGLUT1 staining in the DG at $40\times$ magnification from C57BL/6J LFD (a), C57BL/6J high-fat diet (HFD) (b), AβPP/PS1 LFD (c), and AβPP/PS1 HFD (d) mice. Scale bar = 50 μm. Average mean density of VGLUT1 staining in the DG (e), CA3 (f), and CA1 (g). *$p < 0.05$, ***$p < 0.001$ C57BL/6J LFD ($n = 11$–13; 1–3 subjects excluded) versus C57BL/6J HFD ($n = 7$–8; 3–4 subjects excluded); ##$p < 0.01$, ###$p < 0.001$ AβPP/PS1 LFD ($n = 6$–7; 4–5 subjects excluded) versus AβPP/PS1 HFD ($n = 11$–12; one subject excluded); §$p < 0.05$, §§$p < 0.01$ AβPP/PS1 LFD ($n = 6$–7) versus C57BL/6J LFD ($n = 11$–13); ‡$p < 0.05$, ‡‡$p < 0.01$, ‡‡‡‡$p < 0.0001$ AβPP/PS1 HFD ($n = 11$–12) versus C57BL/6J HFD ($n = 7$–8); where n refers to the number of animals.

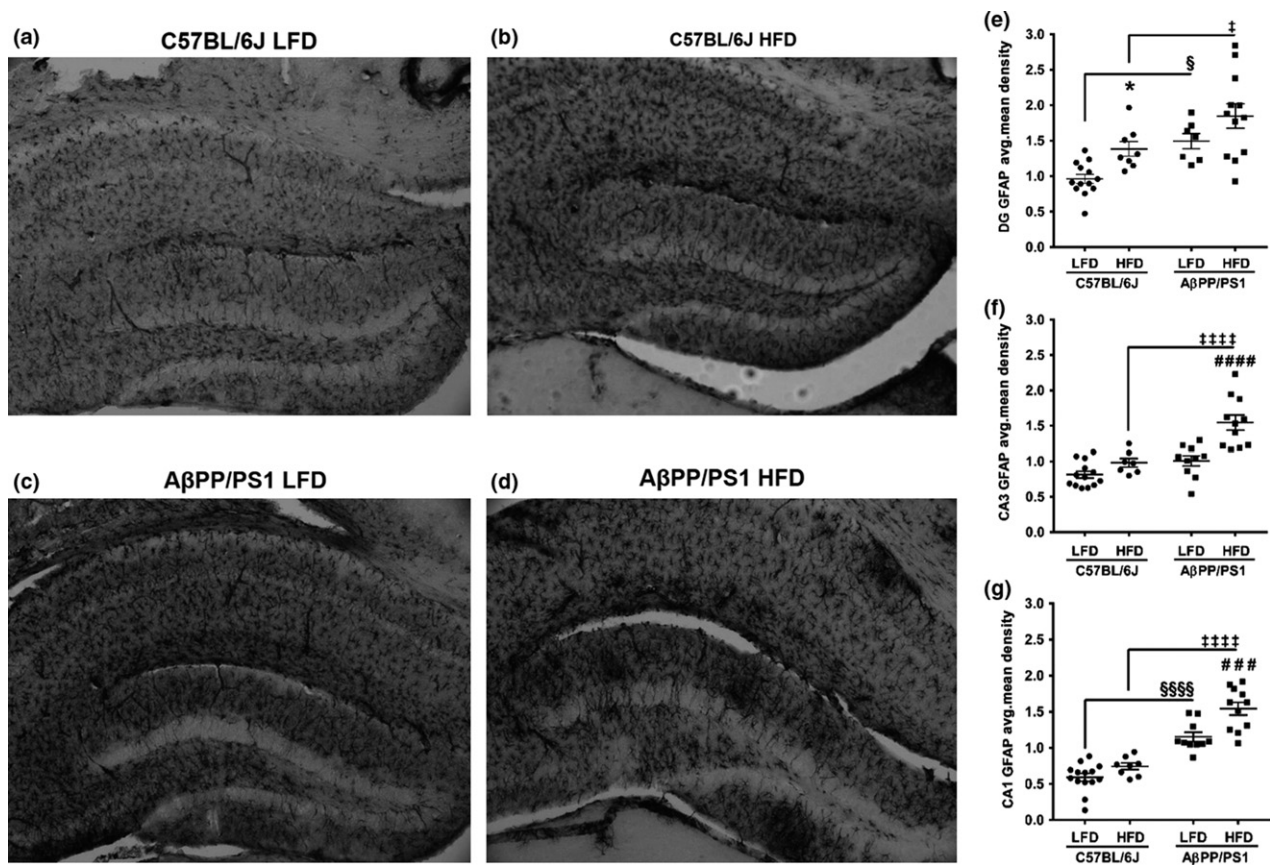**Fig. 6** Glial fibrillary acidic protein (GFAP) immunohistochemistry. Whole hippocampal representative images of GFAP staining in C57BL/6J LFD (a), C57BL/6J high-fat diet (HFD) (b), AβPP/PS1 LFD (c), and AβPP/PS1 HFD (d) mice at 10× magnification. Average mean density of GFAP staining in the DG (e), CA3 (f), and CA1 (g). *$p < 0.05$ C57BL/6J LFD ($n = 13$–14; one subject excluded) versus C57BL/6J HFD ($n = 7$–8; 3–4 subjects excluded); ###$p < 0.001$, ###$p < 0.0001$ AβPP/PS1 LFD ($n = 7$–10, 1–4 subjects excluded) versus AβPP/PS1 HFD ($n = 11$–12; 1 subject excluded); §$p < 0.05$, §§§§$p < 0.0001$ AβPP/PS1 LFD ($n = 7$–10) versus C57BL/6J LFD ($n = 13$–14); ‡$p < 0.05$, ‡‡‡‡$p < 0.0001$ AβPP/PS1 HFD ($n = 11$–12) versus C57BL/6J HFD ($n = 7$–8); where n refers to the number of animals.

Discussion

Half of AD cases are attributable to modifiable lifestyle factors (Barnes and Yaffe 2011) including obesity-induced T2DM that has been suggested to increase the risk for developing AD 1.5- to 2-fold (Allen *et al.* 2004; Ott *et al.* 1999; Arvanitakis *et al.* 2004). While the exact molecular events linking T2DM to AD have not been fully elucidated, the metabolic hypothesis of AD (Hoyer 2002) which supports impaired insulin signaling initiates a series of events including Aβ accumulation (Farris *et al.* 2003),

plaque accumulation ($F[1, 16] = 1410.0$; $p < 0.0001$). However, a diet effect was not observed ($F[1, 16] = 0.1096$; $p = 0.7449$), indicating that a HFD does not increase plaque deposition in AβPP/PS1 mice. This was further supported by ELISA determination in a separate cohort of mice showing a genotype effect ($F[1, 24] = 49.95$; $p < 0.0001$), but not a diet effect ($F[1, 24] = 0.79$; $p = 0.3828$).

neuroinflammation (Granic *et al.* 2009), oxidative stress (De Felice and Ferreira 2014), and calcium dyshomeostasis (Zhang *et al.* 2017) leading to AD pathogenesis. The results of the present study support addition of elevated hippocampal glutamatergic signaling to this growing body of molecular parallels.

In the present study, starting at 3 months of age, C57BL/6J and AβPP/PS1 mice were placed on either LFD (10% kcal from fat) or HFD (60% kcal from fat) with matching protein and sucrose content. Mice fed a HFD developed an obese phenotype starting 1 month after diet initiation and continued until study completion. Since insulin sensitivity is positively correlated with increased longevity and health span in vertebrates (Arum *et al.* 2014), we choose to examine peripheral blood glucose clearance in these mice. The obese phenotype resulted in impaired peripheral insulin signaling and glucose tolerance as observed in the ipITT and ipGTT. The insulin resistance observed in the HFD mouse groups explains the elevated 15 h fasting blood glucose
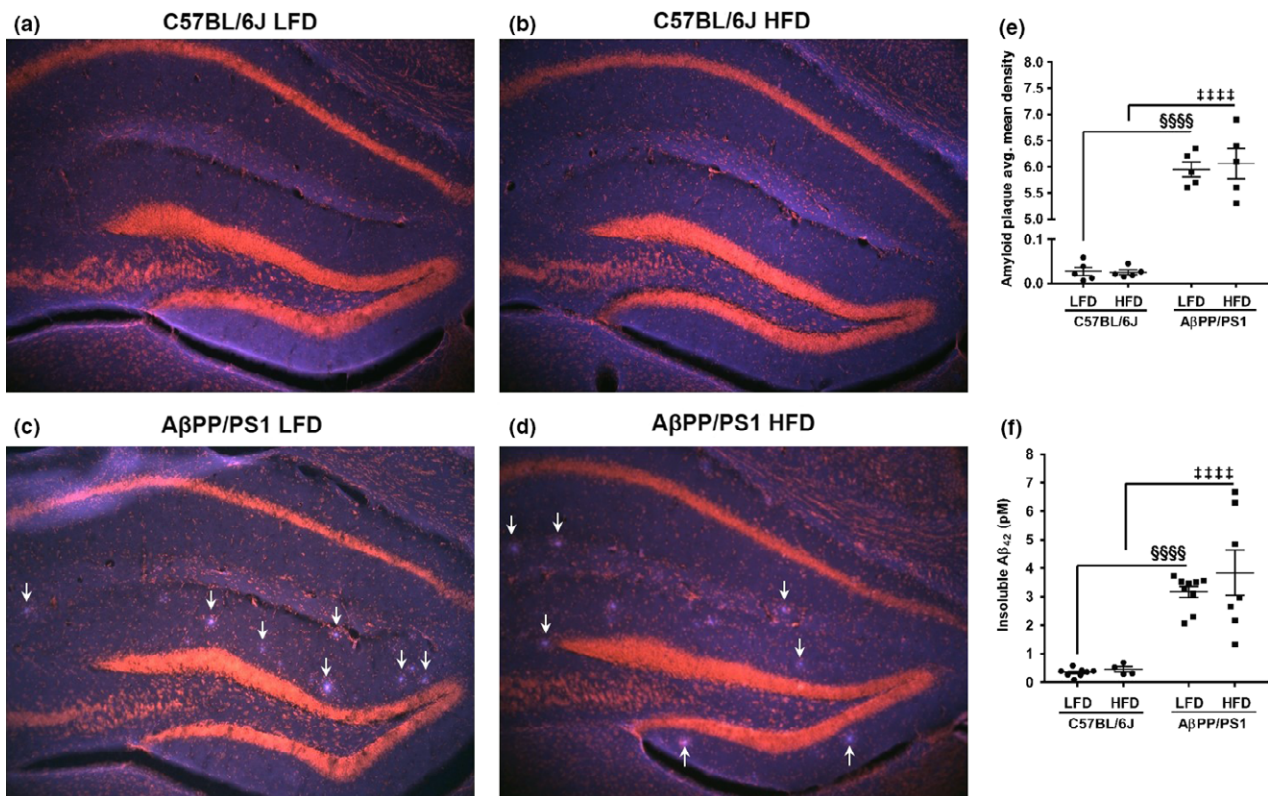
Fig. 7 Amyloid Plaque Formation. Whole hippocampal representative images of amyloid plaque formation (blue) and nuclei staining (red) by EtBr in C57BL/6J LFD (a), C57BL/6J high-fat diet (HFD) (b), AβPP/PS1 LFD (c), and AβPP/PS1 HFD (d) mice at 10× magnification. Arrows indicate plaque formations in (c) and (d). Average mean density of plaque formation in the hippocampus (e) and insoluble Aβ$_{42}$ ELISA determination (f). $^{§§§§}p < 0.0001$ AβPP/PS1 LFD ($n = 5,9$) versus C57BL/6J LFD ($n = 5,8$); $^{‡‡‡‡}p < 0.0001$ AβPP/PS1 HFD ($n = 5,7$) versus C57BL/6J HFD ($n = 5,4$), where n refers to the number of animals and seven subjects per group were excluded from IHC plaque analysis.

levels compared to genotype-matched LFD groups. Interestingly, AβPP/PS1 mice fed a LFD had a similar metabolic profile to HFD mice supporting a naturally occurring insulin resistance in these mice, which has been reported elsewhere (Pedrós *et al.* 2014; Macklin *et al.* 2017). Despite the innate insulin resistance observed in AβPP/PS1 mice, HFD led to a further disruption of their metabolic profile.

A HFD has been shown to negatively affect learning and memory in cognitively normal rodents (Kanoski and Davidson 2011; Cordner and Tamashiro 2015) as well as exacerbate cognitive decline and AD-related neuropathology in animal models (Vandal *et al.* 2014; Knight *et al.* 2014; Thériault *et al.* 2016; Julien *et al.* 2010). For this study, diet treatments began prior to the onset of typically reported AD-related pathology and continued through an age when pathology and plaque burden are well developed in the AβPP/PS1 mouse model. During the visible portion (Day 1) of the MWM behavioral task, similar performances in the latency to the platform and cumulative distance traveled from the platform were observed in all groups of mice, indicating comparable visual acuity and physical activity despite weight

differences. Learning impairments in AβPP/PS1 mice were discerned during the second training day with the hidden escape platform. Throughout the training blocks, we observed that a higher percentage of C57BL/6J LFD and HFD mice successfully navigate the MWM while traveling less distance from the platform. To the contrary, AβPP/PS1 mice presented with learning impairments that were worsened when fed a HFD as supported by 1) a slower escape latency and 2) the cumulative distance from the submerged escape platform during the first two training blocks. By the third training block, AβPP/PS1 performance was similar to that observed during the Day 1 visible platform, but no significant improvements were observed. However, during the MWM probe challenge on the third day, no differences in the number of annulus 40 crossing was observed. The MWM paradigm employed in this study, while atypical from previously published reports from our laboratory (Hascup and Hascup 2015), was designed to reduce stress and anxiety in the mouse. The visible platform on Day 1 helped to habituate mice to the novel pool environment while testing for visual acuity since some inbred mouse strains develop retinal degeneration

(Chang *et al.* 2002). Furthermore, the shorter training duration avoided learning limitations from multiple practice sessions, prevented fatigue, and increased throughput (Alamed *et al.* 2006). These data support that a HFD can negatively affect learning in both C57BL/6J and AβPP/PS1 mice.

Glutamate, the predominant excitatory neurotransmitter in the mammalian CNS, plays an essential role in learning and memory (Riedel *et al.* 2003) and has been implicated in several neurodegenerative disorders including Huntington's, Parkinson's, and Alzheimer's diseases. To measure glutamate, we used an enzyme-based MEA with high spatial resolution (50×100 μm recording sites) that allowed for independent measures from the DG, CA3, and CA1 dorsal hippocampus, a region that is important for consolidation and retrieval of spatial memory during the MWM task (Cimadevilla *et al.* 2005). In the present study, AβPP/PS1 LFD mice exhibited elevated basal glutamate (CA1) and stimulus-evoked glutamate release (DG, CA3, and CA1) compared to C57BL/6J LFD mice. The elevated basal glutamate may result from a combination of mechanisms affecting soluble $A\beta_{42}$ levels that are known to elicit glutamate release (Hascup and Hascup 2016; Talantova *et al.* 2013). First, the transgene expressions in AβPP/PS1 result in progressive $A\beta_{42}$ accumulation (Alley *et al.* 2010), and second, the insulin resistance observed in these mice may prevent IDE from degrading monomeric $A\beta_{42}$ leading to further accumulation and overactivation of α7nAChR on presynaptic glutamatergic terminals. Since hippocampal tissue was used for IHC, none was available for biochemical analysis. Further studies examining soluble $A\beta_{42}$ are needed in order to validate this hypothesis.

VGLUT1, the predominant subtype of vesicles that store hippocampal glutamate (Liguz-lecznar and Skangiel-kramska 2007), was increased in the CA3 and CA1 of AβPP/PS1 LFD compared to C57BL/6J LFD mice. Increased expression of VGLUT1 has been demonstrated to cause excess glutamate release (Daniels *et al.* 2011); however, homeostatic mechanisms exist to limit aberrant synaptic firing that may arise from environmental or genetic variations. But, during the early stages of AD, it is hypothesized that these negative feedback mechanisms begin to destabilize in cortical and hippocampal regions (Frere and Slutsky 2018). For example, epileptiform spikes have been observed in both AβPP/PS1 mice (Minkeviciene *et al.* 2009) and amnestic mild cognitively impaired patients (Vossel *et al.* 2013) as well as hyperexcitability of CA1 pyramidal neurons in AβPP/PS1 mice (Šišková *et al.* 2014). This hyperexcitability coupled with the increased VGLUT1 expression may explain the increased stimulus-evoked glutamate release observed throughout the hippocampus of the present study.

Both C57BL/6J and AβPP/PS1 mice fed a HFD presented with elevated basal (CA3 and CA1) and stimulus-evoked glutamate release (DG and CA1) compared to genotype-matched LFD mice. As described above, the increased extracellular glutamate observed in AβPP/PS1 HFD mice may be explained by the accumulation of $A\beta_{42}$ stimulating glutamate release, but this would not be the case in C57BL/6J HFD mice. However, a HFD would initiate a cascade of separate events in both genotypes leading to the increased basal and stimulus-evoked glutamate release. The insulin resistance and subsequent increase in circulating blood glucose levels observed in both HFD mice would lead to an increase in neuronal glucose accumulation. Since neuronal glutamate synthesis can be derived from glucose (Sonnewald 2014), the higher blood glucose levels would increase the neurotransmitter pool of glutamate, which is supported by the elevated VGLUT1 density observed in the DG, CA3, and CA1 of HFD mice.

A HFD can up-regulate glial glutamate transporter expression while increasing the maximal velocity of clearance (Valladolid-Acebes *et al.* 2012). While the present study did not examine EAAT density, increased expression of GFAP is indicative of astrogliosis (Brahmachari *et al.* 2006) that is associated with an increase in glial glutamate transporters in response to chronic cerebral injuries and neurodegenerative disorders (Haroon *et al.* 2017). At first, this appears counterintuitive. More transporters support faster glutamate clearance that would decrease basal and evoked glutamate concentrations. But, elevated glutamate release causes increased EAAT density as a mechanism to prevent chronic accumulation of extracellular glutamate and potential excitotoxicity (Munir *et al.* 2000). Although not significant in all hippocampal subregions, stimulus-evoked glutamate uptake was increased in AβPP/PS1 LFD versus diet-matched C57BL/6J mice and a HFD further increased these rates in the DG and CA3. In other words, glutamate uptake rate generally increased in response to increases in basal and stimulus-evoked glutamate release.

As expected, hippocampal plaque pathology was only observed in AβPP/PS1 mice; however, a HFD did not increase plaque density which is similar to previous reports in these mice (Thériault *et al.* 2016). This may be due to the astrogliotic response to control plaque deposition in the pathogenesis of AD (Kraft *et al.* 2013). As such, we observed increased hippocampal GFAP density in AβPP/PS1 LFD and HFD compared to diet-matched C57BL/6J control mice that did not present with plaque pathology. GFAP density throughout the hippocampus was further elevated in AβPP/PS1 HFD compared to LFD mice, but this was only mildly observed in the DG of C57BL/6J HFD mice. Since astroglia play a role in Aβ clearance (Ries and Sastre 2016), the elevated astrogliotic inflammatory response, particularly in AβPP/PS1 HFD mice, may have prevented additional plaque accumulation.

The elevated extracellular hippocampal glutamate levels observed in C57BL/6J HFD as well as AβPP/PS1 LFD and HFD mice would contribute to their decreased performance

on the MWM task reported here and elsewhere (Thériault *et al.* 2016). The NMDA receptor is important for spatial learning and memory tasks (Morris *et al.* 1986), but mild, chronic overactivation would be detrimental to synaptic plasticity. This argument is based on the signal-to-noise hypothesis of NMDA receptor activation. Elevated tonic glutamate levels (as observed in this study) prevent the detection of phasic signals thereby blocking formation of new learning (Parsons *et al.* 2007). This process could occur over an extended period of time before calcium overload, excitotoxicity, and eventual neurodegeneration as observed in AD. As such, this mechanism helps to explain the cognitive-improving effects of memantine, an NMDA receptor antagonist, in some AD patients (Parsons *et al.* 2007). In support of this, AβPP/PS1 mice fed a HFD followed by treatment with memantine saw significant reductions in insulin resistance, neuroinflammation, and cognitive deficits (Ettcheto *et al.* 2018). Alternatively, a HFD has been shown to decrease NMDA receptor subunit GluN2B leading to desensitization that may account for cognitive deficits (Valladolid-Acebes *et al.* 2012).

The concentration of extracellular basal glutamate is debated throughout the scientific literature with reports ranging from nanomolar to micromolar concentrations (Herman and Jahr 2007; Burmeister *et al.* 2013; Messam *et al.* 1995). These discrepancies are frequently attributed to methodological considerations that often times yield similar results when additional factors are taken into consideration. The size of our MEA recording sites limits our recording capabilities to the extracellular matrix (ECM) where we are measuring glutamate release and clearance from multiple synapses. As such, a summation of multiple extrasynaptic spillover events may cause elevated levels compared to those reported using patch clamp techniques in slice preparations. Additionally, the diffusion capabilities of neurotransmitters and other membrane impermeable molecules in the ECM are subject to both volume fraction ($\alpha = 0.2$) and tortuosity ($\lambda = 1.6$) (Syková and Nicholson 2008). The α effectively amplifies the concentration of extrasynaptic spillover of glutamate in the ECM while the λ simultaneously slows down its diffusion and uptake into high-affinity transporters. Furthermore, the depolarizing stimulus used in the present study creates a positive net charge on the ECM resulting in a drag effect on the negatively charged glutamate molecules (Gundelfinger *et al.* 2010) and changes the membrane potential which EAATs rely upon for efficient uptake of glutamate (Takahashi *et al.* 1997). The net effect is a slower clearance of stimulus-evoked glutamate release when compared to other methods. Of course, tissue damage is always a concern with any invasive technique including, but not limited to, slice preparations, microdialysis, and MEA recordings. However, the ceramic substrate (Al_2O_3) on the MEAs used in this study have good biocompatibility helping to limit CNS damage allowing for single-unit neuronal activity measurements for at least 6 months post-implantation

(Hascup *et al.* 2009). The MEAs employed in this study have routinely demonstrated that basal extracellular glutamate are sensitive to Na^+-channel (tetrodotoxin), Ca^{2+}-channel (ω-conotoxin), and EAAT (DL-*threo*-β-Benzyloxyaspartic acid) blockade lending credence to a healthy parenchyma surrounding the implanted MEA (Hascup *et al.* 2010; Hascup and Hascup 2016; Hascup *et al.* 2007). Furthermore, the extracellular glutamate concentrations reported in this manuscript fall below the Km (~20 μM) for EAATs (Zhou and Danbolt 2013). Moreover, basal hippocampal glutamate concentrations for C57BL/6J LFD mice (~1 μM) are below the reported EC_{50} (3.7 μM) for the NR1/NR2B NMDA receptor (Banke and Traynelis 2003), further strengthening our premise that chronic overactivation of NMDA receptors, as observed in the HFD and AβPP/PS1 groups would be detrimental to synaptic plasticity, cognition, and may lead to eventual neurodegeneration. Regardless, the current study was not designed to be a definitive assessment of basal glutamate concentrations. In fact, the level of basal glutamate is dependent on a number of criteria including transporter density (Herman and Jahr 2007), ECM developmental stage (Gundelfinger *et al.* 2010), and the glia–neuron ratio (Azevedo *et al.* 2009) resulting in marked variation between brain regions, maturation, and species (Burmeister *et al.* 2013).

Conclusion

Excitotoxicity is a proposed mechanism underlying the neurodegeneration associated with AD. However, the basal and stimulus-evoked glutamate release values reported here are not considered neurotoxic for an intact nervous system. Rather, the current study (when combined with previous research from our laboratory) highlights a consistent theme of elevated hippocampal glutamate starting as early as 2–4 months in AβPP/PS1 mice (Hascup and Hascup 2015) that is potentially mediated by soluble $A\beta_{42}$ (Hascup and Hascup 2016). Furthermore, obesity-induced insulin resistance caused cognitive impairments and increased extracellular glutamate in AβPP/PS1 mice. The progressive deposition of $A\beta_{42}$ with AD progression may chronically elevate glutamate leading to the cognitive and function decline observed in AD, which can be exacerbated by modifiable lifestyle factors such as obesity-induced insulin resistance. While additional studies are ongoing to elucidate mechanisms associated with dietary influences on glutamate dynamics in AβPP/PS1 mice, hippocampal glutamate levels may serve as a viable early therapeutic biomarker for AD pathogenesis.

Acknowledgments and conflict of interest disclosure

Author contributions

KNH conceived the study, conducted the experiments, analyzed the data, and wrote the manuscript. SOB assisted with experiments and data analysis. MKR performed the IHC and corresponding data analysis. HAB supervised IHC and revised the manuscript. YF and AB performed the ELISA, assisted with data analysis, and revised the manuscript. ERH conceived and supervised the study and revised the manuscript. All authors approved the final version of the manuscript.

Open science badges

This article has received a badge for *Open Materials* and for *Open Data* because it made the data publicly available. The data can be accessed at https://doi.org/10.13140/rg.2.2. 11180.10888 and https://osf.io/5whvu (figures for data) and https://osf.io/gd5vf (materials and methods). The complete Open Science Disclosure form for this article can be found at the end of the article. More information about the Open Practices badges can be found at https://cos.io/our-services/ open-science-badges/.

References

Alamed J., Wilcock D. M., Diamond D. M., Gordon M. N. and Morgan D. (2006) Two-day radial-arm water maze learning and memory task; robust resolution of amyloid-related memory deficits in transgenic mice. *Nat. Protoc.* **1**, 1671–1679.

Allen K. V., Frier B. M. and Strachan M. W. J. (2004) The relationship between type 2 diabetes and cognitive dysfunction: longitudinal studies and their methodological limitations. *Eur. J. Pharmacol.* **490**, 169–175.

Alley G. M., Bailey J. A., Chen D., Ray B., Puli L. K., Tanila H., Banerjee P. K. and Lahiri D. K. (2010) Memantine lowers amyloid-beta peptide levels in neuronal cultures and in APP/PS1 transgenic mice. *J. Neurosci. Res.* **88**, 143–154.

Arum O., Boparai R. K., Saleh J. K., Wang F., Dirks A. L., Turner J. G., Kopchick J. J., Liu J.-L., Khardori R. K. and Bartke A. (2014) Specific suppression of insulin sensitivity in growth hormone receptor gene-disrupted (GHR-KO) mice attenuates phenotypic features of slow aging. *Aging Cell* **13**, 981–1000.

Arvanitakis Z., Wilson R. S., Bienias J. L., Evans D. A. and Bennett D. A. (2004) Diabetes mellitus and risk of Alzheimer disease and decline in cognitive function. *Arch. Neurol.* **61**, 661–666.

Azevedo F. A. C., Carvalho L. R. B., Grinberg L. T., Farfel J. M., Ferretti R. E. L., Leite R. E. P., Jacob Filho W., Lent R. and Herculano-Houzel S. (2009) Equal numbers of neuronal and nonneuronal cells make the human brain an isometrically scaled-up primate brain. *J. Comp. Neurol.* **513**, 532–541.

Banke T. G. and Traynelis S. F. (2003) Activation of NR1/NR2B NMDA receptors. *Nat. Neurosci.* **6**, 144–152.

Barnes D. E. and Yaffe K. (2011) The projected effect of risk factor reduction on Alzheimer's disease prevalence. *Lancet. Neurol.* **10**, 819–828.

Boger H. A., Middaugh L. D., Patrick K. S., Ramamoorthy S., Denehy E. D., Zhu H., Pacchioni A. M., Granholm A.-C. and McGinty J. F. (2007) Long-term consequences of methamphetamine exposure in young adults are exacerbated in glial cell line-derived neurotrophic factor heterozygous mice. *J. Neurosci.* **27**, 8816–8825.

Brahmachari S., Fung Y. K. and Pahan K. (2006) Induction of glial fibrillary acidic protein expression in astrocytes by nitric oxide. *J. Neurosci.* **26**, 4930–4939.

Burmeister J. J. and Gerhardt G. A. (2001) Self-referencing ceramic-based multisite microelectrodes for the detection and elimination of interferences from the measurement of L-glutamate and other analytes. *Anal. Chem.* **73**, 1037–1042.

Burmeister J. J., Moxon K. and Gerhardt G. A. (2000) Ceramic-based multisite microelectrodes for electrochemical recordings. *Anal. Chem.* **72**, 187–192.

Burmeister J. J., Pomerleau F., Palmer M., Day B. K., Huettl P. and Gerhardt G. A. (2002) Improved ceramic-based multisite microelectrode for rapid measurements of L-glutamate in the CNS. *J. Neurosci. Methods* **119**, 163–171.

Burmeister J. J., Davis V. A., Quintero J. E., Pomerleau F., Huettl P. and Gerhardt G. A. (2013) Glutaraldehyde cross-linked glutamate oxidase coated microelectrode arrays: selectivity and resting levels of glutamate in the CNS. *ACS Chem. Neurosci.* **4**, 721–728.

Chang B., Hawes N. L., Hurd R. E., Davisson M. T., Nusinowitz S. and Heckenlively J. R. (2002) Retinal degeneration mutants in the mouse. *Vision. Res.* **42**, 517–525.

Cimadevilla J. M., Miranda R., López L. and Arias J. L. (2005) Partial unilateral inactivation of the dorsal hippocampus impairs spatial memory in the MWM. *Brain Res. Cogn. Brain Res.* **25**, 741–746.

Cordner Z. A. and Tamashiro K. L. K. (2015) Effects of high-fat diet exposure on learning & memory. *Physiol. Behav.* **152**, 363–371.

Cummings J. L., Morstorf T. and Zhong K. (2014) Alzheimer's disease drug-development pipeline: few candidates, frequent failures. *Alzheimers. Res. Ther.* **6**, 37.

Daniels R. W., Miller B. R. and DiAntonio A. (2011) Increased vesicular glutamate transporter expression causes excitotoxic neurode generation. *Neurobiol. Dis.* **41**, 415–420.

De Felice F. G. and Ferreira S. T. (2014) Inflammation, defective insulin signaling, and mitochondrial dysfunction as common molecular denominators connecting type 2 diabetes to Alzheimer disease. *Diabetes* **63**, 2262–2272.

Ettcheto M., Sánchez-López E., Gómez-Mínguez Y., Cabrera H., Busquets O., Beas-Zarate C., García M. L., *et al.* (2018) Peripheral and central effects of memantine in a mixed preclinical mice model of obesity and familial Alzheimer's disease. *Mol. Neurobiol.* **55**, 7327–7339.

Fang Y., McFadden S., Darcy J., Hill C. M., Huber J. A., Verhulst S., Kopchick J. J., Miller R. A., Sun L. Y. and Bartke A. (2017) Differential effects of early-life nutrient restriction in long-lived GHR-KO and normal mice. *GeroScience* **39**, 347–356.

Farrand A. Q., Helke K. L., Gregory R. A., Gooz M., Hinson V. K. and Boger H. A. (2017) Vagus nerve stimulation improves locomotion and neuronal populations in a model of Parkinson's disease. *Brain Stimul.* **10**, 1045–1054.

Farris W., Mansourian S., Chang Y., Lindsley L., Eckman E. A., Frosch M. P., Eckman C. B., Tanzi R. E., Selkoe D. J. and Gue S. (2003) Insulin-degrading enzyme regulates the levels of insulin, amyloid beta-protein, and the beta amyloid precursor protein intracellular domain in vivo. *Proc. Natl Acad. Sci. USA* **100**, 4162–4167.

De Felice F. G. (2013) Alzheimer's disease and insulin resistance: translating basic science into clinical applications. *J. Clin. Invest.* **123**, 531–539.

Frere S. and Slutsky I. (2018) Alzheimer's disease: from firing instability to homeostasis network collapse. *Neuron* **97**, 32–58.

Gallagher M., Burwell R. and Burchinal M. (2015) Severity of spatial learning impairment in aging: development of a learning index for performance in the Morris water maze. *Behav. Neurosci.* **129**, 540–548.

Godyń J., Jończyk J., Panek D. and Barbara M. (2016) Therapeutic strategies for Alzheimer's disease in clinical trials. *Pharmacol. Reports* **68**, 127–138.

Granic I., Dolga A. M., Nijholt I. M., van Dijk G. and Eisel U. L. M. (2009) Inflammation and NF-κB in Alzheimer's disease and diabetes. *J. Alzheimer's Dis.* **16**, 809–821.

Gulinello M., Gertner M., Mendoza G., Schoenfeld B. P., Oddo S., LaFerla F., Choi C. H., McBride S. M. J. and Faber D. S. (2009) Validation of a 2-day water maze protocol in mice. *Behav. Brain Res.* **196**, 220–227.

Gundelfinger E. D., Frischknecht R., Choquet D. and Heine M. (2010) Converting juvenile into adult plasticity: a role for the brain's extracellular matrix. *Eur. J. Neurosci.* **31**, 2156–2165.

Haroon E., Miller A. H. and Sanacora G. (2017) Inflammation, glutamate, and glia: a trio of trouble in mood disorders. *Neuropsychopharmacology* **42**, 193–215.

Hascup K. N. and Hascup E. R. (2015) Altered neurotransmission prior to cognitive decline in AβPP/PS1 mice, a model of Alzheimer's disease. *J. Alzheimer's Dis.* **44**, 771–776.

Hascup K. N. and Hascup E. R. (2016) Soluble amyloid-β42 stimulates glutamate release through activation of the α7 nicotinic acetylcholine receptor. *J. Alzheimer's Dis.* **53**, 337–347.

Hascup K. N., Rutherford E. C., Quintero J. E., Day B. K., Nickell J. R., Pomerleau F., Huettl P., Burmeister J. J. and Gerhardt G. A. (2006) Second-by-second measures of L-glutamate and other neurotransmitters using enzyme-based microelectrode arrays, in *Electrochemical Methods for Neuroscience - NCBI Bookshelf, in Electrochem. Methods Neurosci* (Borland A. C. and Michael L. M., eds), pp. 407–450. CRC Press.

Hascup K. N., Hascup E. R., Pomerleau F., Huettl P. and Gerhardt G. A. (2007) Second-by-second measures of L-glutamate in the prefrontal cortex and striatum of freely moving mice. *J. Pharmacol. Exp. Ther.* **324**, 725–731.

Hascup E. R., af Bjerkén S., Hascup K. N., Pomerleau F., Huettl P., Strömberg I. and Gerhardt G. A. (2009) Histological studies of the effects of chronic implantation of ceramic-based microelectrode arrays and microdialysis probes in rat prefrontal cortex. *Brain Res.* **1291**, 12–20.

Hascup E. R., Hascup K. N., Stephens M., Pomerleau F., Huettl P., Gratton A. and Gerhardt G. A. (2010) Rapid microelectrode measurements and the origin and regulation of extracellular glutamate in rat prefrontal cortex. *J. Neurochem.* **115**, 1608–1620.

Hascup K. N., Hascup E. R., Stephens M. L., Glaser P. E. A., Yoshitake T., Mathé A. A., Gerhardt G. A. and Kehr J. (2011) Resting glutamate levels and rapid glutamate transients in the prefrontal cortex of the Flinders Sensitive Line rat: a genetic rodent model of depression. *Neuropsychopharmacology* **36**, 1769–1777.

Hascup K. N., Hascup E. R., Littrell O. M. *et al.* (2013) in *Microelectrode Array Fabrication and Optimization for Selective Neurochemical Detection, in Microelectrode Biosens*, Vol. 80, (Marinesco S. and Dale N., eds), pp. 27–54. Humana Press, Totowa, NJ.

Hascup K. N., Lynn M. K., Fitzgerald P. J., Randall S., Kopchick J. J., Boger H. A., Bartke A. and Hascup E. R. (2016) Enhanced cognition and hypoglutamatergic signaling in a growth hormone receptor knockout mouse model of successful aging. *J. Gerontol. A Biol. Sci. Med. Sci.* **72**, 329–337.

Herman M. A. and Jahr C. E. (2007) Extracellular glutamate concentration in hippocampal slice. *J. Neurosci.* **27**, 9736–9741.

Holland W. L., Brozinick J. T., Wang L.-P., Hawkins E. D., Sargent K. M., Liu Y., Narra K., *et al.* (2007) Inhibition of Ceramide Synthesis Ameliorates Glucocorticoid-, Saturated-Fat-, and Obesity-Induced Insulin Resistance. *Cell Metab.* **5**, 167–179.

Hoyer S. (2002) The brain insulin signal transduction system and sporadic (type II) Alzheimer disease: an update. *J. Neural. Transm.* **109**, 341–360.

Jack C. R., Knopman D. S., Jagust W. J., Petersen R. C., Weiner M. W., Aisen P. S., Shaw L. M., *et al.* (2013) Tracking pathophysiological processes in Alzheimer's disease: an updated hypothetical model of dynamic biomarkers. *Lancet. Neurol.* **12**, 207–216.

Janson J., Laedtke T., Parisi J. E., O'Brien P., Petersen R. C. and Butler P. C. (2004) Increased risk of type 2 diabetes in Alzheimer disease. *Diabetes* **53**, 474–481.

Jin M. and Selkoe D. J. (2015) Systematic analysis of time-dependent neural effects of soluble amyloid β oligomers in culture and in vivo: prevention by scyllo-inositol. *Neurobiol. Dis.* **82**, 152–163.

Julien C., Tremblay C., Phivilay A., Berthiaume L., Émond V., Julien P. and Calon F. (2010) High-fat diet aggravates amyloid-beta and tau pathologies in the 3xTg-AD mouse model. *Neurobiol. Aging* **31**, 1516–1531.

Kanoski S. E. and Davidson T. L. (2011) Western diet consumption and cognitive impairment: links to hippocampal dysfunction and obesity. *Physiol. Behav.* **103**, 59–68.

Knight E. M., Martins I. V. A., Gümüsgöz S., Allan S. M. and Lawrence C. B. (2014) High-fat diet-induced memory impairment in triple-transgenic Alzheimer's disease (3xTgAD) mice is independent of changes in amyloid and tau pathology. *Neurobiol. Aging* **35**, 1821–1832.

Kraft A. W., Hu X., Yoon H., *et al.* (2013) Attenuating astrocyte activation accelerates plaque pathogenesis in APP/PS1 mice. *FASEB J.* **27**, 187–198.

Liguz-lecznar M. and Skangiel-kramska J. (2007) Vesicular glutamate transporters (VGLUTs): the three musketeers of glutamatergic system. *Acta. Neurobiol. Exp.*, **67**, 207–2018.

Macklin L., Griffith C. M., Cai Y., Rose G. M., Yan X.-X. and Patrylo P. R. (2017) Glucose tolerance and insulin sensitivity are impaired in APP/PS1 transgenic mice prior to amyloid plaque pathogenesis and cognitive decline. *Exp. Gerontol.* **88**, 9–18.

Messam C. A., Greene J. G., Greenamyre J. T. and Robinson M. B. (1995) Intrastriatal injections of the succinate dehydrogenase inhibitor, malonate, cause a rise in extracellular amino acids that is blocked by MK-801. *Brain Res.* **684**, 221–224.

Minkeviciene R., Rheims S., Dobszay M. B., Zilberter M., Hartikainen J., Fulop L., Penke B., *et al.* (2009) Amyloid -induced neuronal hyperexcitability triggers progressive epilepsy. *J. Neurosci.* **29**, 3453–3462.

Moloney A. M., Griffin R. J., Timmons S., O'Connor R., Ravid R. and O'Neill C. (2010) Defects in IGF-1 receptor, insulin receptor and IRS-1/2 in Alzheimer's disease indicate possible resistance to IGF-1 and insulin signalling. *Neurobiol. Aging* **31**, 224–243.

Morris R. G., Anderson E., Lynch G. S. and Baudry M. (1986) Selective impairment of learning and blockade of long-term potentiation by an N-methyl-D-aspartate receptor antagonist, AP5. *Nature* **319**, 774–776.

Mota S. I., Ferreira I. L. and Rego A. C. (2014) Dysfunctional synapse in Alzheimer's disease – A focus on NMDA receptors. *Neuropharmacology* **76**, 16–26.

Munir M., Correale D. M. and Robinson M. B. (2000) Substrate-induced up-regulation of Na(+)-dependent glutamate transport activity. *Neurochem. Int.* **37**, 147–162.

Ott A., Stolk R. P., vanHarskamp F., Pols H. A., Hofman A. and Breteler M. M. (1999) Diabetes mellitus and the risk of dementia: the rotterdam study. *Neurology* **53**, 1937–1942.

Parsons C. G., Stöffler A. and Danysz W. (2007) Memantine: a NMDA receptor antagonist that improves memory by restoration of homeostasis in the glutamatergic system–too little activation is bad, too much is even worse. *Neuropharmacology* **53**, 699–723.

Paxinos G. and Franklin K. B. J. (2004) *The Mouse Brain in Stereotaxic Coordinates*. Professional Publishing, Gulf.

Pedrós I., Petrov D., Allgaier M., Sureda F., Barroso E., Beas-Zarate C., Auladell C., *et al.* (2014) Early alterations in energy metabolism in the hippocampus of APPswe/PS1dE9 mouse model of Alzheimer's disease. *Biochim. Biophys. Acta* **1842**, 1556–1566.

Riedel G., Platt B. and Micheau J. (2003) Glutamate receptor function in learning and memory. *Behav. Brain Res. Brain Res.* **140**, 1–47.

Ries M. and Sastre M. (2016) Mechanisms of Aβ clearance and degradation by glial cells. *Front. Aging Neurosci.* **8**, 160.

Šišková Z., Justus D., Kaneko H., Friedrichs D., Henneberg N., Beutel T., Pitsch J., *et al.* (2014) Dendritic structural degeneration is functionally linked to cellular hyperexcitability in a mouse model of Alzheimer's disease. *Neuron* **84**, 1023–1033.

Sonnewald U. (2014) Glutamate synthesis has to be matched by its degradation - where do all the carbons go? *J. Neurochem.* **131**, 399–406.

Syková E. and Nicholson C. (2008) Diffusion in brain extracellular space. *Physiol. Rev.* **88**, 1277–1340.

Takahashi M., Billups B., Rossi D., Sarantis M., Hamann M. and Attwell D. (1997) The role of glutamate transporters in glutamate homeostasis in the brain. *J. Exp. Biol.* **200**, 401–409.

Talantova M., Sanz-Blasco S., Zhang X., Xia P., Akhtar M. W., Okamoto S., Dziewczapolski G., *et al.* (2013) Aβ induces astrocytic glutamate release, extrasynaptic NMDA receptor activation, and synaptic loss. *Proc. Natl. Acad. Sci. U. S. A.* **110**, E2518–E2527.

Talbot K., Wang H.-Y., Kazi H., Han L.-Y., Bakshi K. P., Stucky A., Fuino R. L., *et al.* (2012) Demonstrated brain insulin resistance in Alzheimer's disease patients is associated with IGF-1 resistance, IRS-1 dysregulation, and cognitive decline. *J. Clin. Invest.* **122**, 1316–1338.

Thériault P., ElAli A. and Rivest S. (2016) High fat diet exacerbates Alzheimer's disease-related pathology in APPswe/PS1 mice. *Oncotarget* **7**, 67808–67827.

Valladolid-Acebes I., Merino B., Principato A., Fole A., Barbas C., Lorenzo M. P., García A., *et al.* (2012) High-fat diets induce changes in hippocampal glutamate metabolism and neurotransmission. *Am. J. Physiol. Endocrinol. Metab.* **302**, E396–E402.

Vandal M., White P. J., Tremblay C., St-Amour I., Chevrier G., Emond V., Lefrançois D., *et al.* (2014) Insulin reverses the high-fat diet-induced increase in brain aβ and improves memory in an animal model of Alzheimer disease. *Diabetes* **63**, 4291–4301.

Vossel K. A., Beagle A. J., Rabinovici G. D., Shu H., Lee S. E., Naasan G., Hegde M., *et al.* (2013) Seizures and epileptiform activity in the early stages of Alzheimer disease. *JAMA Neurol.* **70**, 1158–1166.

Yang T., Li S., Xu H., Walsh D. M. and Selkoe D. J. (2017) Large soluble oligomers of amyloid β-protein from Alzheimer brain are far less neuroactive than the smaller oligomers to which they dissociate. *J. Neurosci.* **37**, 152–163.

Zhang S., Chai R., Yang Y.-Y., Guo S.-Q., Wang S., Guo T., Xu S.-F., Zhang Y.-H., Wang Z.-Y. and Guo C. (2017) Chronic diabetic states worsen Alzheimer neuropathology and cognitive deficits accompanying disruption of calcium signaling in leptin-deficient APP/PS1 mice. *Oncotarget* **8**, 43617–43634.

Zhao W.-Q. and Townsend M. (2009) Insulin resistance and amyloidogenesis as common molecular foundation for type 2 diabetes and Alzheimer's disease. *Biochim. Biophys. Acta* **1792**, 482–496.

Zhou Y. and Danbolt N. C. (2013) GABA and glutamate transporters in brain. *Front Endocrinol. (Lausanne).* **4**, 165.